Earth and Planetary Science Letters 452 (2016) 60–68

Contents lists available at ScienceDirect

Earth and Planetary Science Letters

www.elsevier.com/locate/epsl

On dislocation glide in $MgSiO_3$ bridgmanite at high-pressure and high-temperature

Antoine Kraych, Philippe Carrez, Patrick Cordier *

Unité Matériaux et Transformations, UMR 8207 CNRS/Université Lille 1, 59655 Villeneuve d'Ascq, France

ARTICLE INFO

Article history:
Received 20 April 2016
Received in revised form 9 July 2016
Accepted 19 July 2016
Available online 5 August 2016
Editor: J. Brodholt

Keywords:
bridgmanite
lower mantle rheology
dislocation glide
kink-pair mechanism

ABSTRACT

Dislocation glide in $MgSiO_3$ bridgmanite with *Pbnm* perovskite structure is modeled at 30 and 60 GPa for the [100](010) and [010](100) slip systems. The velocity of screw dislocations is calculated in the thermally activated regime based on the kink-pair mechanism. We show that the dislocation velocity determination can rely on the atomic scale calculations of a limited amount of parameters: the Peierls stress τ_p, and the formation enthalpy of a single kink H_k. From the dislocation velocities, the evolution of stress as a function of temperature can be derived from the Orowan equation at any strain rate. Calculations performed at laboratory strain-rates of 10^{-5} s^{-1} reproduce well the high stress levels found experimentally. This demonstrates the influence of lattice friction in the mechanical properties of bridgmanite. The same calculations are performed at mantle strain-rate (10^{-16} s^{-1}). They demonstrate that in the lower mantle, bridgmanite would always be in the thermally activated regime and that stresses close to 1 GPa are still necessary to move dislocations in bridgmanite. In the uppermost lower mantle, dislocation glide is inhibited and other deformation mechanisms, involving diffusion, are needed.

1. Introduction

Mantle convection is elusive at human timescale since it operates over hundreds of million years. Seismic anisotropy, which samples the direction-dependence of elastic wave propagation, represents one of the potential observables of past convection since it is an indicator of flow patterns in the deep Earth through the development of Crystal Preferred Orientations (CPO) (Montagner, 1994; Mainprice, 2007). Robust evidences for seismic anisotropy have been reported in the upper mantle and in the transition zone as well as in the lowermost lower mantle (i.e. in the D" layer). By contrast, a consensus has developed that the lower mantle at depths between 700 and 2700 km is mostly isotropic (Meade et al., 1995; Panning and Romanowicz, 2006) although some average radial anisotropy has recently been reported by de Wit and Trampert (2015). From the mineral physics point of view, this raises the question of the deformation mechanism of lower mantle phases. Plastic deformation by dislocation creep induces crystal rotation and may produce CPO. More specifically, dislocation creep in its commonly accepted sense (Weertman, 1955) involves two deformation mechanisms (see also Boioli et al., 2015 for quantification in olivine): (i) dislocation glide which is usually the most efficient strain producing mechanism and which produces shear and hence crystal rotation; (ii) dislocation climb which is usually (in metals, but also in olivine as shown by Boioli et al., 2015) a recovery mechanism and induces no crystal rotation. Dislocation glide is thus the mechanism to assess in order to evaluate the possibility of CPO to develop. The ability of MgO to deform by dislocation glide under lower mantle conditions has been studied recently (Cordier et al., 2012; Amodeo et al., 2015; Marquardt and Miyagi, 2015). Here we focus on the possibility of activating dislocation glide in bridgmanite. Deforming bridgmanite experimentally is challenging given the pressure needed. In the first compression experiments performed at ambient temperature (Meade and Jeanloz, 1990; Merkel et al., 2003), no texture development was observed. Some more recent experiments suggest however indications of slip after transformation from San Carlos olivine in a diamond anvil cell (Wenk et al., 2004; Miyagi, 2009) and from multianvil deformation experiments (Cordier et al., 2004; Miyajima et al., 2009). Recently, the first shear deformation experiments at lower mantle conditions of bridgmanite and magnesiowüstite aggregates were reported by Girard et al. (2016). However, no information on deformation mechanisms or texture development was obtained from this study.

* Corresponding author. Tel.: +33 320 434341.
E-mail address: patrick.cordier@univ-lille1.fr (P. Cordier).

http://dx.doi.org/10.1016/j.epsl.2016.07.035

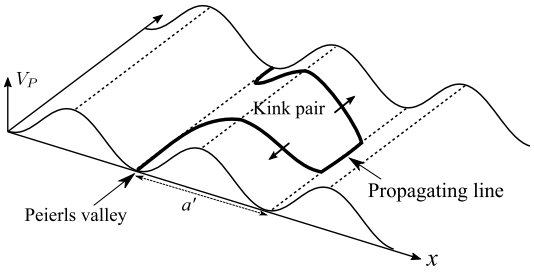

Fig. 1. Schematic of the thermally activated glide process of a dislocation overcoming the Peierls potential via a kink-pair mechanism.

In this work, we aim to determine the efficiency of dislocation glide in the pure $MgSiO_3$ end-member bridgmanite at conditions (P, T, $\dot{\varepsilon}$) relevant to the lower mantle. We rely on atomic scale calculations to model dislocation glide at high-pressure and temperature. Being based on a modeling of the deformation mechanisms (and not on extrapolation of empirical laws) our calculations are able to account for geological strain rates that are impossible to reach experimentally. Previous studies have assessed lattice friction of various slip systems in $MgSiO_3$ bridgmanite based on the Peierls–Nabarro model (Ferré et al., 2007; Gouriet et al., 2014). From theses studies, it turns out that [100](010) and [010](100) are the easiest glide systems. This was recently confirmed by atomistic calculations of dislocation core structures (Hirel et al., 2014). In the present study, atomistic calculations are expanded and used to address the evolution of the critical shear stress associated with dislocation glide of these slip systems at finite temperature. Our aim is to show that multiscale modeling of dislocation glide is able, with no adjustable parameter to reproduce experimental data obtained at high-pressure and temperature conditions. Moreover, this approach is unique in allowing to extend these calculations to low strain-rates with no extrapolations, hence providing the first rheological data for bridgmanite under lower mantle conditions.

2. Methodology

In high lattice friction material such as bridgmanite, a dislocation has to overpass an energy barrier V_p (the Peierls potential) in order to move. At 0 K, a dislocation can only move in response to the applied stress and the minimum stress required to trigger glide scales on the spatial derivative of V_p (Peierls, 1940). We refer to such critical stress as the Peierls stress τ_p. In other words, τ_p can also be seen as a purely mechanical measurement of the lattice friction. At finite temperature however, the dislocation does not overpass the Peierls potential as a rigid straight line, but through a thermally activated mechanism involving the nucleation and the propagation of kink-pairs (Fig. 1). Under the action of thermal fluctuations, a part of the dislocation can bulge over the Peierls potential. With the help of stress, the bulge (described as a pair of kinks) can reach a critical size beyond which it expands freely, leading to the propagation of the dislocation into the next Peierls valley. Assuming that the nucleation event corresponds to the limiting process (as commonly observed in metals and ionic materials, including archetype of perovskites such as $SrTiO_3$; see for instance the work of Castillo-Rodriguez and Sigle, 2011), any dependence of the critical nucleation enthalpy ΔH^* for kink-pair nucleation on the applied stress τ can be expressed through the following relationship (Kocks et al., 1975):

$$\Delta H^*(\tau) = 2H_k\left(1-\left(\frac{\tau}{\tau_p}\right)^p\right)^q \tag{1}$$

where H_k corresponds to the enthalpy of a single kink ($2H_k$ stands thus for the formation of a kink-pair) and τ_p to the Peierls stress.

Table 1
Structural and elastic parameters of $MgSiO_3$ bridgmanite computed at 30 and 60 GPa.

	$P = 30$ GPa	$P = 60$ GPa
a (Å)	4.65	4.54
b (Å)	4.76	4.66
c (Å)	6.72	6.56
$\mu_{[100]}$ (GPa)	179.6	206.3
$\mu_{[010]}$ (GPa)	177.8	208.0

In Eq. (1), p and q are parameters that control the rate of decrease of the critical enthalpy from $2H_k$ at $\tau \to 0$, down to zero when $\tau = \tau_p$.

In a thermally activated regime described through the kink-pair mechanism, the corresponding dislocation velocity $v(\tau, T)$ can be evaluated according to a classical Boltzmann expression (Eq. (2)) highlighting the influence of the temperature on the kink-pair nucleation probability. It should be mentioned here that ΔH^*, is usually independent of T (Schoeck, 1965).

$$v(\tau, T) = v_0 \exp\left(\frac{-\Delta H^*(\tau)}{kT}\right) \tag{2}$$

In Eq. (2), v_0 corresponds to a pre-exponential term depending on geometrical constants as explained in the following.

Combining Eq. (2) with the Orowan equation which links the strain rate $\dot{\varepsilon}$ to the dislocation density ρ of dislocations with Burgers vector b gliding at a velocity $v(\tau, T)$, it turns out that the critical stress for dislocation glide can be written according to the following relationship:

$$\tau = \tau_p\left(1-\left(C\frac{T}{H_k}\right)^{1/q}\right)^{1/p} \tag{3}$$

where C depends on the investigated strain rate and on the nature of the dislocation (in particular on the modulus of the Burgers vector, and on some geometrical factors describing the slip geometry). It is however remarkable that the evolution of the critical stress as a function of temperature is fully constrained by a limited number of parameters, the Peierls stress τ_p, the single kink enthalpy H_k and the set of (p, q) parameters capturing the evolution of the kink-pair nucleation enthalpy as a function of the applied stress. In the following, the parameters τ_p and H_k are computed using atomistic calculations and we use a so-called kink–kink interaction model (Seeger and Schiller, 1962) in order to determine the couple (p, q) for a given dislocation and its associated slip plane.

3. Results

3.1. Atomistic calculation of single kink enthalpy H_k

3.1.1. Computational details

Throughout this study, molecular statics calculations are used to model the atomic configurations of straight and kinked dislocations in $MgSiO_3$ bridgmanite. Calculations are performed at two different pressures, 30 and 60 GPa characteristic of the upper part of the Earth's lower mantle. The inter-atomic potential (Oganov et al., 2000) used as well as the minimization procedure as implemented in the LAMMPS package (Plimpton, 1995) are described in Hirel et al. (2014) and Krayche et al. (2016). The lattice parameters of bridgmanite, computed at 30 and 60 GPa, are listed in Table 1 as well as the corresponding shear modulus for [100] and [010] dislocations. Atomic kink configurations are determined by minimizing the energy of a simulation cell containing a dipole of kink-bearing dislocations (Fig. 2). The system size is chosen to be large enough to allow a full relaxation of the kink. A typical system size involves therefore more than 10^6 atoms. Although the relaxed configuration

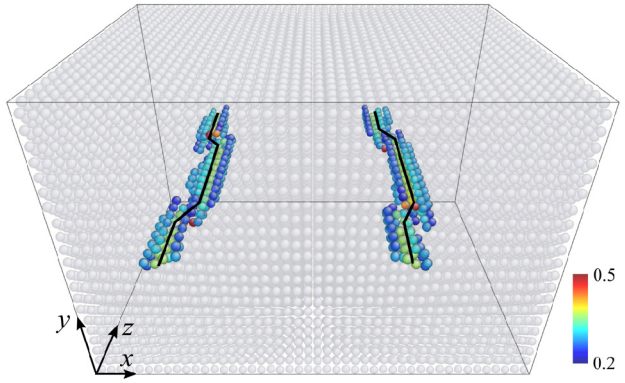

Fig. 2. Typical simulation system used to compute the enthalpy of kinks. Simulation cell (of length $23c \times 22b \times 24a$) contains a dipole of screw dislocations (here of Burgers vector [100]). Each dislocation exhibits a kink-pair along the z direction. For sake of visualization, only magnesium atoms are displayed. Atoms in the vicinity of the dislocation cores are colored according to a central-symmetry criteria. (For interpretation of the references to color in this figure, the reader is referred to the web version of this article.)

Table 2
Summary of key properties for screw dislocations of [100](010) and [010](100) slip systems. Peierls stresses are taken from Hirel et al. (2014). The projected length λ of an isolated kink is given in units of b. H_k corresponds to the single kink enthalpy. Dimensionless parameters (p, q) describe the evolution of the nucleation kink-pair enthalpy as a function of stress (see text for details).

	[100](010)		[010](100)	
	$P = 30$ GPa	$P = 60$ GPa	$P = 30$ GPa	$P = 60$ GPa
τ_p (GPa)	4.9	9.0	4.5	10.8
H_k (eV)	9.5	10.2	5.9	10.7
$H_k/\mu b^3$	0.084	0.085	0.049	0.081
λ	3.3	4.5	3.8	3.3
p, q	0.5, 1.0	0.53, 1.45	0.59, 2.32	0.55, 1.71

of isolated kinks can be achieved in a finite system, the single kink energy, extracted from atomistic calculations, has to be corrected from the elastic interaction between kinks.

3.1.2. Application to single kinks on screw dislocation cores of Burgers vector [100] and [010]

Kinks configurations are modeled for [100] screw dislocation in (010), and [010] screw dislocations in (100). The kink profiles are plotted in Fig. 3. Their structures have been extracted from the atomistic calculations by computing the evolution of the disregistry along the dislocation line across the glide plane. A quantitative analysis of the kink spreading along the dislocation line (spatial coordinate z, see Fig. 2) has been performed by fitting the diregistries with respect to the following expression (Joós and Zhou, 2001):

$$f_k(z) = \frac{2a'}{\pi} \arctan\left(\exp\left(\frac{\pi z}{\lambda b}\right)\right) \tag{4}$$

In Eq. (4), λ can be viewed as a measurement of the spreading of an isolated kink of height a'. The corresponding values of λ for the four kinks investigated are given in Table 2. It is worth noticing that for the four configurations, the kinks are widely spread with $\lambda > 3$.

The values of H_k for the different glide systems are listed in Table 2. For [100](010) at 30 and 60 GPa, the kink enthalpies are close to 10 eV. The increase of pressure has a small influence on the reduced expression $H_k/\mu b^3$ showing that the increase of H_k with pressure is mostly driven by the pressure dependence of the elastic constants. In case of [010](100), we find a stronger effect of pressure on the kink enthalpy as H_k increases from 6 eV at 30 GPa

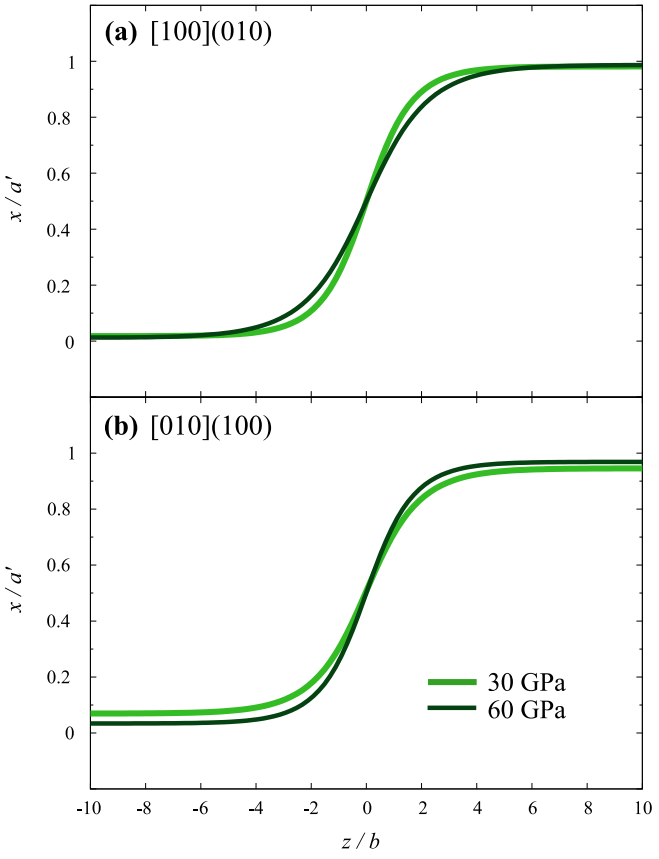

Fig. 3. Kink profiles at 30 and 60 GPa for (a) [100] screw dislocation in (010), (b) [010] screw dislocation in (100). Coordinates x and z correspond respectively to the glide direction and the dislocation line (as indicated in Fig. 2).

to 10 eV at 60 GPa, which is not entirely due to elasticity as shown by the evolution of the $H_k/\mu b^3$ ratio in Table 2.

3.2. Atomistic evaluation of the Peierls stress τ_p

3.2.1. Computational details

As mentioned in the Methods section, the Peierls stress corresponds to the minimum stress required to move a dislocation in absence of thermal activation. It corresponds therefore to a purely mechanical measurement of the lattice friction borne by a dislocation. Classically, Peierls stress investigations at atomic scale rely on a computational system containing one straight dislocation on which an appropriate simple shear strain is applied to maximize the shear stress in the glide plane. The applied shear strain is then incrementally increased with a force minimization procedure being applied at each increment. Then monitoring the disregistry allows precise determination of the stress required to move the dislocation in the absence of temperature. The corresponding Peierls stress is thus determined from the derivative of the system's potential energy with respect to the shear displacements. This procedure has been applied to bridgmanite in Hirel et al. (2014). However, the Peierls stress can also be determined by computing directly the lattice friction through the computation of the Peierls potential V_p. Such calculations involve the computation of the Minimum Energy Path (MEP) between two stable positions of the dislocation core in the bridgmanite lattice. MEP can be accurately determined from Nudged Elastic Band (NEB) algorithms. In this study, NEB calculations are performed to compute the MEP for [100] and [010] dislocations in respectively (010) and (100) at 60 GPa. The NEB allows to determine dislocation transitory configurations and their energies, by relaxing atomic configurations

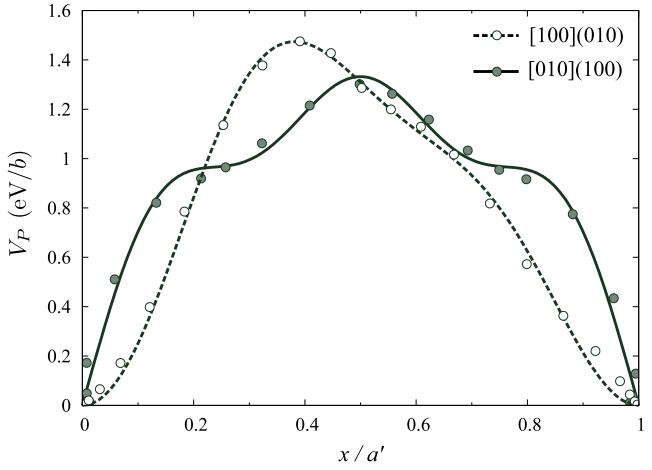

Fig. 4. Peierls potential V_p computed at 60 GPa from NEB calculations for [100] screw dislocation in (010) and [010] screw dislocation in (100). The Peierls potential is plotted as a function of the dislocation position between two adjacent Peierls valleys.

with respects to the inter-atomic forces, and to artificial spring forces binding the transitory configurations together (Jónsson et al., 1998). For a complete overview of the simulation cells and calculation procedures, we refer to Krayche et al. (2016).

3.2.2. *Peierls stress and lattice friction as a function of pressure*

The Peierls potential of [100](010) and [010](100) screw dislocations at 60 GPa are plotted in Fig. 4. For [100](010) slip system, the Peierls potential for the screw component is highly asymmetric. Such asymmetry in V_p was already observed at 30 GPa. It results from the glide mechanism of the dislocation itself. During its glide, the dislocation core exhibits an unstable structure which involves spreading up to the formation of two fractional dislocations (Schoeck, 2001). During motion, the leading fractional dislocation starts to move while the other remains immobile (Fig. 5). When the leading fractional dislocation has reached the next stable position, the tailing fractional dislocation starts to glide until it reaches the other one at its final position. One may notice that such a glide mechanism occurs at 30 and 60 GPa, with however a noticeable increase of the energy barrier at 60 GPa. Indeed, the maximum values of the Peierls potential are 1.17 eV/b at 30 GPa, and 1.48 eV/b at 60 GPa.

In contrast to [100](010), the Peierls potential for [010](100) is symmetric with a maximum value of 1.3 eV/b at 60 GPa. The intrinsic lattice resistance of (100) to plastic shear is therefore slightly lower than the one of (010). The glide mechanism of [010] dislocations shows similarities with the one of the [100] dislocations. Here again, dislocation glide involves a fractionated process. It occurs however in two steps (Fig. 5). The two fractional dislocations move first, one by one, at midway, and secondly toward the next stable position. As a consequence of this two stages behavior, no asymmetry is observed on V_p.

The Peierls stress τ_p can be calculated from the spatial derivative of the Peierls potential according to $\tau_p \cdot b = \{dV_p/dx\}_{max}$. At 60 GPa, Peierls stresses deduced from Fig. 4 for [100](010) and [010](100) are thus 7.5 GPa and 9.2 GPa respectively. Compared to τ_p computed from direct application of shear strain (Hirel et al., 2014), such derivation of V_p tends to slightly underestimate the Peierls stress. However, it is important to point out that the present calculation of V_p does not account for the sensitivity of the Peierls potential to the applied stress (see for instance Krayche et al., 2016). As a consequence, the following relies on Peierls stresses reported in Hirel et al. (2014) as summarized Table 2.

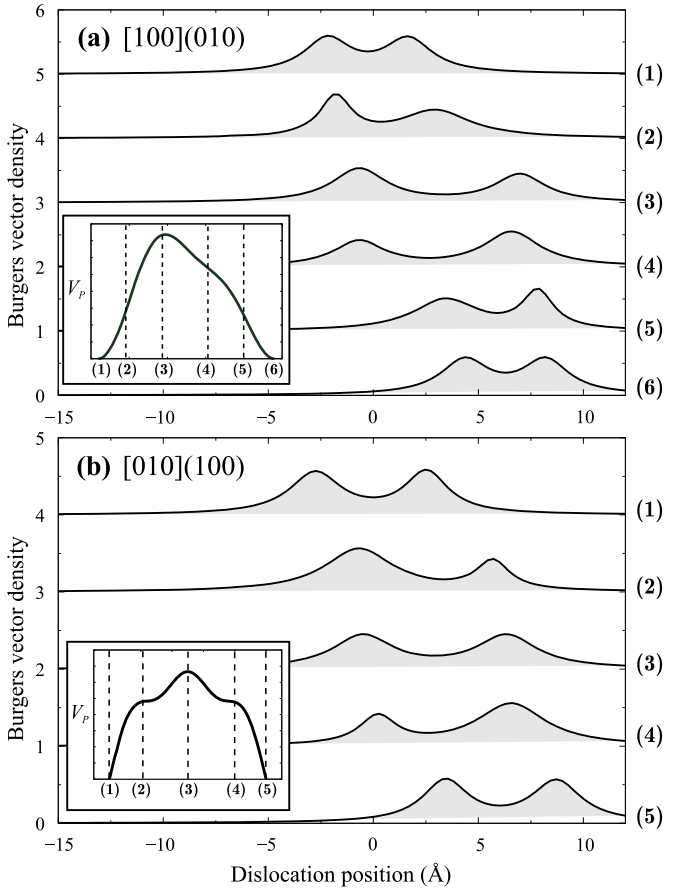

Fig. 5. Variation of the dislocation structure during its glide. The dislocation structure is plotted through the density of Burgers vector, i.e. the derivative of the disregistry function. (a) Density of Burgers vector for a [100] dislocation gliding in (010) at 60 GPa, with the associated Peierls potential. (b) Density of Burgers vector for a [010] dislocation gliding in (100) at 60 GPa, with the associated Peierls potential.

3.3. *Critical nucleation enthalpy of kink-pair at low stress*

Since we determine the energy of an isolated kink, it is possible to model the nucleation of kink-pairs under an applied stress. At low stress, the kink-pair is composed by two kinks of height a', distant from each other by a width w. Increasing the stress, the width between kinks will necessary decrease to finally reach a narrow bulge configuration at high stress. For a kink-pair of width w larger than its height a', Seeger and Schiller (1962) proposed a long-range interaction model to determine the kink-pair critical nucleation enthalpy. The total kink-pair formation enthalpy ΔH is the sum of the enthalpies of two individual kinks and of their interaction energy. The latter is proposed to be inversely proportional to the separation distance w, as for two electrical point charges (see also Caillard and Martin, 2003). Under stress, the nucleation enthalpy is given by Eq. (5) where the last term corresponds to the work of the applied stress.

$$\Delta H(\tau, w) = 2H_k - \alpha\mu b^2 \frac{a'^2}{w} - \tau b a' w \tag{5}$$

The second term in Eq. (5) corresponds to the long-range interaction between kinks. α is a constant related to the intensity of the "coulombic" interaction between kinks, and the factor μb^2 is introduced for the sake of dimensionality. As demonstrated in the Appendix, the use of an Elastic Interaction model, as proposed by Koizumi et al. (1993, 1994), allows to validate our choice of relying on the kink–kink interaction model (Eq. (5)) for bridgmanite with

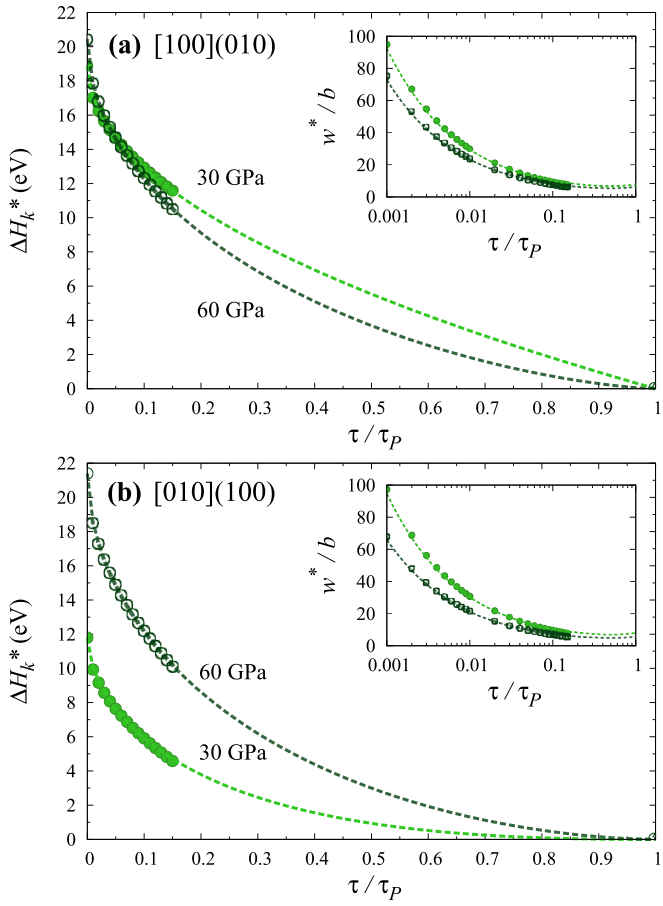

Fig. 6. Critical nucleation enthalpy for kink-pair mechanism plotted as a function of the applied stress at 30 and 60 GPa for (a) [100] screw dislocation in (010) and (b) [010] screw dislocation in (100). Inserts show the evolution of the critical width between kinks as a function of stress.

a single constant α equal to 0.17 for both slip systems [010](100) and [100](010).

From Eq. (5), the critical (labeled by "$*$") kink-pair configuration is obtained by minimizing the nucleation enthalpy with respect to the variable width w. A straightforward calculation leads to the following dependencies for the critical configuration width w^* (Eq. (6)) and the associated critical nucleation enthalpy ΔH^* (Eq. (7)).

$$w^* = \sqrt{\frac{\alpha \mu b a'}{\tau}} \tag{6}$$

$$\Delta H^*(\tau) = 2H_k - \sqrt[3]{a'b} \cdot \sqrt{2\alpha\mu\tau} \tag{7}$$

According to Eq. (7), introducing values of H_k computed at the atomic scale, we can further calculate the evolution of ΔH^* as a function of the applied stress for the four cases of interest as shown in Fig. 6. The constraints of ΔH^* at low stress combined with the knowledge of the Peierls stress enables to fit the parameters (p, q) of Eq. (1). We report in Table 2 the results of the adjustment procedure for the two investigated slip systems. For [010](100), one may notice the strong increase of the kink-pair nucleation enthalpy as the pressure increases from 30 to 60 GPa.

3.4. Critical resolved shear stress for [100] and [010] dislocations in bridgmanite

According to Eq. (3), the critical resolved shear stresses for dislocations gliding in (010) and (100) can be determined using the relevant parameters taken from Table 2. It should be nevertheless stressed that a given imposed strain rate has to be defined as it directly imposes the value of the C factor appearing in Eq. (3). Assuming that the critical stress corresponds to the minimal stress required to promote the dislocation motion according to the kink-pair mechanism, we can further show that C will be directly related to the imposed strain rate and the geometry of the slip. Based on the seminal work of Dorn and Rajnak (1964), for a given strain rate $\dot{\varepsilon}$, C can be rewritten as:

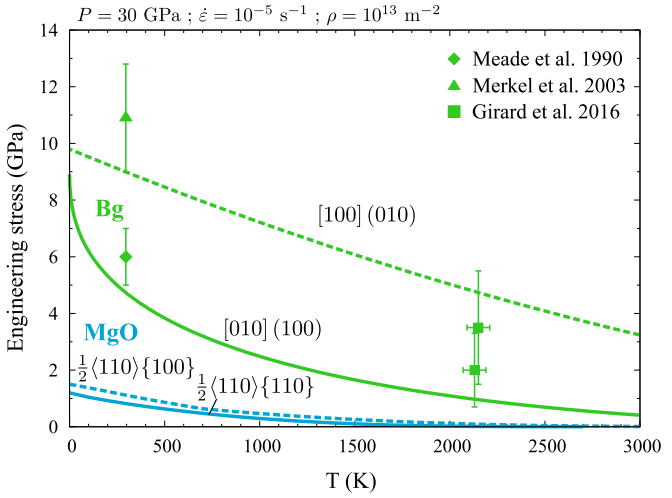

Fig. 7. Stress evolution as a function of temperature, for glide of [100] and [010] dislocation in bridgmanite (Bg) under a strain rate of 10^{-5} s^{-1}. In order to compare with experimental data coming from polycrystalline deformation experiments, we define a first order engineering stress corresponding to twice of the critical resolved shear stress, i.e. meaning that we maximize the Schmid factor. Results of present modeling are compared with experimental available data for bridgmanite (symbols), and numerical study of $1/2\langle 110\rangle\{110\}$ and $1/2\langle 110\rangle\{100\}$ dislocations glide in periclase (MgO) taken from Amodeo et al. (2012).

$$C = \frac{k}{2} \ln\left(\frac{\nu_D a' b^2}{2w^{*2}} \frac{\sqrt{\rho}}{\dot{\varepsilon}} \right) \tag{8}$$

where ν_D stands for the Debye frequency (calculated as 3×10^{13} s^{-1} in this material), w^* resulting from Eq. (6) describes the bow-out configuration of the kink-pair mechanism operating on a dislocation of Burgers b gliding by incremental step a'. Taken through a logarithm, the sensitivity of w^* to the stress is negligible and one can assume a typical constant value of $10b$ for w^*. Thus, C is much more constrained by the choice of a dislocation density ρ and of a given strain rate $\dot{\varepsilon}$.

For a typical laboratory strain rate of 10^{-5} s^{-1}, we use a dislocation density of 10^{13} m^{-2} as reported in Miyajima et al. (2009). Within such conditions, $C = 1.34 \times 10^{-3}$ eV/K and the evolution of the critical resolved shear stress for the two slip systems of interest is reported in Fig. 7. For further comparisons with experimental data of the strength of bridgmanite, we translate our calculations into an engineering stress corresponding to the critical resolved shear stress divided by 1/2, i.e. the maximum value of a Schmid factor.

For mantle convection, a typical value for the strain rate of 10^{-16} s^{-1} is considered (Forte and Mitrovica, 2001) with a dislocation density of 10^8 m^{-2}. Therefore, for Earth's mantle conditions, C becomes 2.18×10^{-3} eV/K. The moderate increase of C resulting from the change of strain rate conditions further confirms that C dependences are largely damped out by the logarithmic formulation. The resulting critical resolved shear stresses are plotted in Fig. 8.

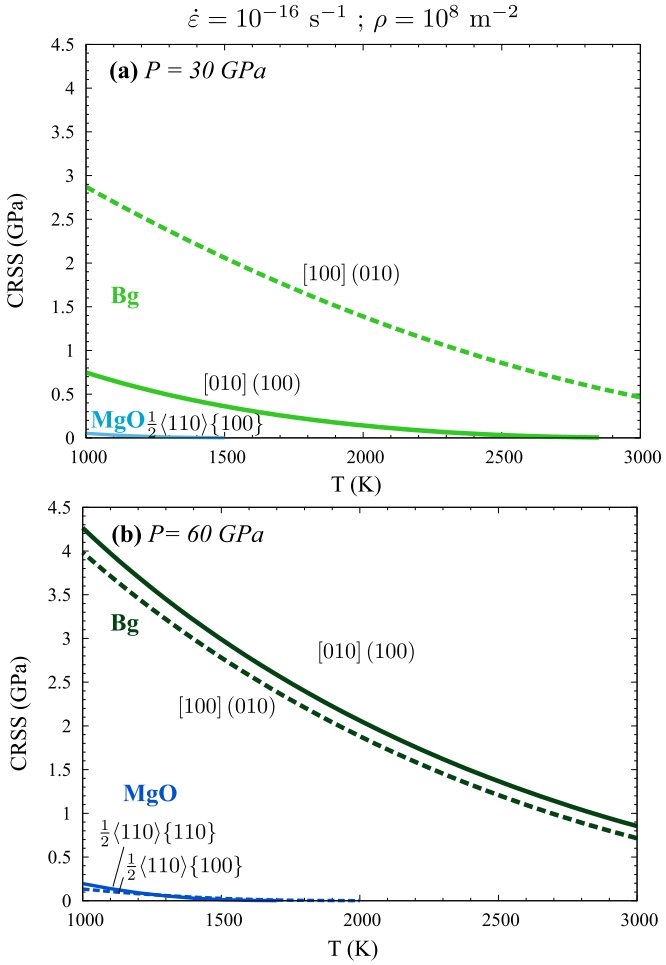

Fig. 8. Critical resolved shear stress evolution as a function of temperature, calculated from the glide of [100] and [010] dislocations in bridgmanite (Bg) at a typical mantle strain rate of 10^{-16} s^{-1}. a) at 30 GPa, b) at 60 GPa. Comparison is provided with the results on the glide of $1/2\langle 110\rangle\{110\}$ and $1/2\langle 110\rangle\{100\}$ dislocations in periclase (MgO) taken from Amodeo et al. (2012) and calculated under the same conditions (in blue). (For interpretation of the references to color in this figure legend, the reader is referred to the web version of this article.)

4. Discussion

In this study, we present an extensive model of dislocation glide in bridgmanite based on multi-scale numerical modeling. This approach combines standard models of dislocation theory which are informed by a few calculations, performed at the atomic scale. It is applied to dislocations from slip systems expected to be the easiest (Ferré et al., 2007; Hirel et al., 2014). Our results are thus aimed at providing a lower bound of the mechanical properties of bridgmanite as long as glide only is concerned. A very important parameter is the core structure of the dislocations, i.e. the atomic arrangement around the dislocation line since it has a paramount influence on the dislocation mobility. This core structure has been determined in previous studies (Hirel et al., 2014). Screw dislocations which are considered here exhibit a rather narrow core ($1.5 \times$ c and $2 \times$ c for [100] and [010] respectively) with however a clear tendency for spreading in a given plane ((010) for [100] dislocations and (100) for [010] dislocations) which constrains the slip plane. We see here that under stress, this spreading gives rise to two well-individualized fractional dislocations. The respective motion of these fractional dislocations play an important role on the glide mechanism and hence on the lattice friction borne by the dislocations. We show that for [100] screw dislocations the fractional dislocations exhibit uncorrelated displacements whereas they move together for [010] screw dislocations. The key question addressed in the present study is nonetheless how the conjugate influence of stress and temperature assist dislocation glide in bridgmanite.

Below a critical temperature often called the "athermal temperature" (e.g. Kubin, 2013), plastic flow is controlled by the intrinsic dislocation glide properties and therefore by the capability to nucleate and propagate a kink-pair on dislocation segments. The conjugate influence of stress and temperature in this regime leads to a decrease of the critical resolved shear stress as the temperature increases. From Eq. (3), the "athermal temperature" can be estimated and corresponds within our notation to H_k/C. H_k values between 5 and 10 eV, as computed in this study, mean that the yield stress would become athermal above 4000 K or even higher as H_k is shown to increase with pressure whereas in the same time, C can be considered as a constant to a good approximation. As a consequence, with respect to the melting temperature of bridgmanite (Stixrude, 2005), dislocation glide in bridgmanite necessarily involves a kink-pair mechanism.

The evaluation of dislocation velocities and thus of the critical shear stress are based on the assumption that kink-pair nucleation (and not migration) represents the limiting step for dislocation motion. This assumption is validated by the atomic kink configurations showing that kinks are widely spread with an extension greater than $3b$ (Table 2). Indeed, for widely spread kinks, according to classical description of kink-pair mechanism (e.g. Joós and Zhou, 2001; Caillard and Martin, 2003), migration energy is at least one order of magnitude lower than nucleation energy. Finally, it is worth to recall that we use a simplified model to further evaluate the evolution of ΔH^* for kink-pairs as a function of stress. The kink–kink interaction model proposed by Seeger and Schiller (1962) used here is known to be valid at low stress. By low stress, one means typically a stress below 25% of the Peierls stress. The critical kink-pair nucleation enthalpies have thus been determined for bridgmanite in this stress range (i.e. between 0 and 3 GPa). Extrapolations to higher stress and therefore lower temperature (Fig. 6) are based on a fitting procedure of parameters (p, q) of Eq. (1). This explains why p parameters are found close to 0.5 whatever the pressure or the slip system investigated. Close to the Peierls stress (or at low temperature), the accuracy of the extrapolations is questionable. At low temperature, it is thus preferable to consider our calculations as lower bound of the critical resolved shear stress. Nevertheless, above a typical temperature of 1500 K, high lattice friction of bridgmanite satisfies the inherent assumptions of a kink–kink interaction model such as proposed by Seeger and Schiller (1962).

Deforming high-pressure phases in mantle-relevant pressure and temperature conditions remains a very challenging issue. Significant progress have been achieved however with the development of the D-DIA (Wang et al., 2003) and of the Rotational Deformation Apparatus (RDA, Yamazaki and Karato, 2001). Pioneering results on transition zone minerals showed high-stress levels, even at high-temperature (Weidner et al., 2001). Recently, Girard et al. (2016) provided the first rheological data for a bridgmanite plus ferropericlase assemblage deformed under uppermost lower mantle conditions. These results provide a possibility to assess the outcome of our theoretical predictions. The exercise is not straightforward. Girard et al.'s data describe the strength of a two-phase polycrystal. The *in situ* measurement of lattice strains provides however information on the respective contribution of individual phases. Still we are here dealing with the mechanical response of bridgmanite grains to tri-axial loading also involving the contribution of grain boundaries. Their experiments, involving large strains may also capture the contribution of strain-hardening. In comparison, we provide information on the onset of dislocation glide. This is the reason why, for the comparison presented in Fig. 7,

we have selected the data of Girard et al. (2016) corresponding to the smallest strains, i.e. before the development of strain hardening. Also, since we calculate resolved shear stresses, we have multiplied our results by the maximum value of the Schmid factor to get a proxy of an engineering stress which is more comparable to the outcome of the experiments. Still, care must be taken in the comparison of these two results which should be regarded as a first-order evaluation only. It appears however remarkable that both approaches lead to the same conclusions that, even at high-temperature, high stress levels are necessary to deform bridgmanite. This consistency strongly suggests that high-lattice friction is the key parameter (not disregarding the possible contribution of other mechanisms) which determines the strength of bridgmanite at laboratory strain-rates, even at high temperature. The comparison between these experiments and theoretical predictions can even go one step further. Girard et al. (2016) gained information on the stress partitioning between bridgmanite and ferropericlase. They show that there is a significant rheology contrast between the two phases, bridgmanite being the stronger. A theoretical approach, similar to the one developed here has been already applied to MgO (Amodeo et al., 2012). MgO results are reported in Figs. 7 and 8 for comparison. Although Amodeo et al. (2012) pointed to a significant hardening of MgO under pressure resulting from increasing lattice friction, we reach the same conclusions as Girard et al. (2016) on the rheology contrast between the two phases as far as dislocation glide is concerned.

All recent experimental investigations performed on the rheology of bridgmanite (Girard et al., 2016) and (ferro)periclase (Marquardt and Miyagi, 2015; Girard et al., 2016) at mantle pressure lead to the conclusion that under pressure these phases are very strong. Our theoretical calculations on MgO (Cordier et al., 2012) and here on bridgmanite are in excellent agreement with these results and demonstrate that the strong pressure increase of lattice friction opposed to dislocation glide is the cause of this behavior. The question is however how much of this strength remains at extremely low strain-rates operating in mantle convection.

At low strain-rates, it is easier to deform a material in the thermally activated regime since thermally activated events (here nucleation of a kink-pair) have more time to occur. This has two consequences: (i) lower stress levels are needed at a given temperature, (ii) the transition temperature to the athermal regime is shifted to lower values. This effect has been well illustrated in our previous study on MgO (Cordier et al., 2012). Extrapolating the results of deformation experiments obtained at laboratory strain-rates to mantle conditions over several orders of magnitude remains extremely speculative if one relies only on empirically-based constitutive equations. However, being based on a physical description of the mechanisms, our calculations are able to describe the mobility of dislocations under mantle strain-rates with no extrapolation.

Here we show that lattice friction is so high that bridgmanite remains always in the thermally activated regime, even at mantle strain-rates. Also, although stresses are smaller than at laboratory strain-rates, they remain at a significant level under mantle conditions. Translated into viscosities, these stresses would lead to values in the range 10^{24}–10^{25} Pa s. The strength of bridgmanite under mantle conditions correlates well with the outcome of seismic tomography which shows that although materials is transported through the transition zone, slabs tend to slow down and even stagnate at different depths, including in the uppermost lower mantle (Fukao et al., 2009). Whether this effect corresponds to a continuous increase from 660 km or to a midmantle jump at about 1000 km is still debated however (Rudolph et al., 2015; King, 2016; Liu and Zhong, 2016). Our results suggest that this strengthening correlates with the fact that a potential deformation mechanism, dislocation glide, is inhibited under those conditions in the volumetric dominant phase of the lower mantle: bridgmanite.

The high viscosities that would result from the sole activation of dislocation glide demonstrate that other mechanisms are at play in the Earth's mantle. The contribution of diffusion creep has been assessed quantitatively recently (Glišovic et al., 2015) showing that it could provide a relevant mechanism provided that the grain size is of the order of a millimetre. Given this limitation, further attention should be paid to other mechanisms. If the grain size remains at the millimetre level or below, the role of grain boundaries should be also assessed. Also, dislocation creep does not involve dislocation glide only, but also climb resulting from the absorption of point defects from dislocations. Since it has been shown recently that electric charges carried by dislocations in bridgmanite provide a strong interaction mechanism with vacancies (Hirel et al., 2016), the potential role of climb on creep in bridgmanite appears to need further attention in the future since it is clear that one of the cited mechanisms must control the rheology of bridgmanite in the lower mantle.

5. Conclusions

The present work provides constraints on dislocation creep of $MgSiO_3$ bridgmanite due to the activation of [100] and [010] dislocations, which are the easiest glide systems. Our model provides mechanical data with no adjustable parameters that are validated by the few deformation experiments that have been performed on $MgSiO_3$ bridgmanite. This confirms that during laboratory experiments, even at high temperature, the rheology of bridgmanite is strongly controlled by the high lattice friction opposed to dislocation glide. When applied to the deformation conditions that prevail in the lower mantle (low strain rate, high pressure and temperature), our calculations predict that dislocation glide in bridgmanite still requires high stress levels. This strengthening of bridgmanite correlates well with the viscosity jump associated with the uppermost lower mantle. However, other mechanisms (intracrystalline or at grain boundaries) involving diffusion must operate to account for the plastic flow of bridgmanite in the lower mantle. More work is needed to quantify these processes.

Acknowledgements

This work was supported by funding from the European Research Council under the Seventh Framework Programme (FP7), ERC grant No. 290424 – RheoMan. Constructive comments made by two anonymous reviewers and the editor helped strengthening the manuscript as well as discussions with several colleagues at the 2016 CIDER summer program.

Appendix A

One of the main issues of this study is to evaluate the nucleation critical enthalpy for a kink-pair, $\Delta H^*(\tau)$. Theoretical description of deformation processes involving the kink-pair mechanism has been successfully applied in a variety of materials, including body-centered cubic metals (Xu and Moriarty, 1998; Proville et al., 2013; Gröger and Vitek, 2013), covalent materials like silicon (Pizzagalli et al., 2008), or ionic materials such as MgO (Amodeo et al., 2012), ceramics or $SrTiO_3$ perovskite (Mitchell et al., 1999; Carrez et al., 2010).

The total energy change due to the nucleation of a kink-pair results from three main contributions according to the following relationship:

$$\Delta H(\tau) = \Delta E_{elas} + \Delta W_P - \Delta W_\tau \tag{A.1}$$

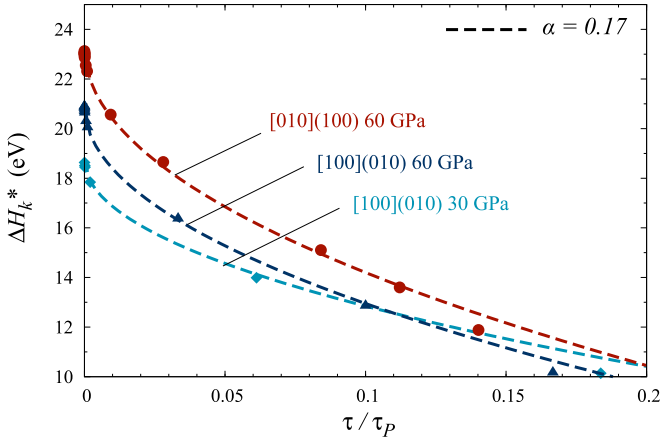

Fig. A.1. Critical nucleation enthalpy of kink-pair $\Delta H^*(\tau)$ of [100] screw dislocation in (010) at 30 and 60 GPa and [010] screw dislocation in (100) at 60 GPa calculated from the (EI) model (filled symbols), with the results (broken line) of the kink–kink interaction model (Eq. (7)). For the kink–kink interaction model, the long-range interaction are computed with $\alpha = 0.17$.

where ΔE_{elas} represents the positive increase of elastic energy associated to the formation a kink-pair, ΔW_P is the energy due to the part of the dislocation lying over the Peierls potential, and W_τ represents the work of the applied stress.

Several models have been proposed to compute this change in enthalpy that has to be supplied by thermal activation to enhance the formation of a pair of kinks (Caillard and Martin, 2003). Most approaches differ only by the mathematical treatment of the change in elastic energy ΔE_{elas} (Suzuki et al., 1995). Indeed, the technical problem relies in the calculation of the elastic energy of the bulge in the dislocation. Koizumi and co-workers (Koizumi et al., 1993) proposed, as an alternative to a double integral over the dislocation line, to discretize the problem into a double sum by considering the continuous curved bulge as a polygon for which the elastic interactions (EI) between segments are well known and available in Hirth and Lothe (1982). A further extension of such discretization to a trapezoidal shape model was then proposed and showed remarkable agreement with a wealth of experimental data (Koizumi et al., 1994; Suzuki et al., 1995). Also, we recently demonstrated that such EI model is able to reproduce experimental data for ionic compounds such as MgO (Amodeo et al., 2012) and satisfies with atomistic calculations in case of bridgmanite $MgSiO_3$ (Krayche et al., 2016).

One remarkable achievement of elastic interaction model based on trapezoidal kink-pair shape is to be not only applicable to low stress region but also to intermediate or even high stresses. Therefore it should satisfy with the so-called line tension model (Dorn and Rajnak, 1964) (at high or intermediate stress) and with kink–kink interaction model at low stress. As pointed out by Seeger and Schiller (1962), at low stresses, long range interaction between isolated kinks dominates the saddle point configuration and associated energy. Therefore, we decide to parameterize the numerical factor α occurring in Eq. (5) accordingly to EI model calculations. Considering the two slip systems [100](010) and [010](100) of bridgmanite and the two typical pressure conditions investigated in this study, we computed the evolution of $\Delta H^*(\tau)$ resulting from the application of EI model (for a complete description of EI model applied to bridgmanite, one may refer to Krayche et al., 2016). Results of EI model are plotted in Fig. A.1. It turns out that for a typical value of $\alpha = 0.17$, whatever the slip system or the investigated pressure, kink–kink interaction model coincides perfectly with EI calculations (Fig. A.1). Since α corresponds to a long-range "coulombic-like" interaction, there is indeed no reason for strong variations between different slip systems in the same material.

The remarkable agreement between the two models is nevertheless restricted to low stress region, i.e. $\tau < 0.25\tau_P$. Above, the solution of kink–kink interaction model follows a square root dependence greatly different from the slope obtained with EI model. This explains why we only rely on the kink-pair model at small stresses and extrapolates the nucleation enthalpy evolution down to zero at the Peierls stress through the use of Eq. (1) which ensure a steeper slope of $\Delta H^*(\tau)$ at higher stress.

References

Amodeo, J., Carrez, Ph., Cordier, P., 2012. Modelling the effect of pressure on the critical shear stress of MgO single crystals. Philos. Mag. 92, 1523–1541. http://dx.doi.org/10.1080/14786435.2011.652689.

Amodeo, J., Schuberth, B.S.A., Bunge, H.-P., Carrez, Ph., Cordier, P., 2015. On the role of thermal heterogeneities on the rheology of MgO under conditions of the Earth's lower mantle. Phys. Earth Planet. Inter. 242, 1–8. http://dx.doi.org/10.1016/j.pepi.2015.02.008.

Boioli, F., Carrez, Ph., Cordier, P., Devincre, B., Marquille, M., 2015. Modeling the creep properties of olivine by 2.5-dimensional dislocation dynamics simulations. Phys. Rev. B 92, 014115. http://dx.doi.org/10.1103/PhysRevB.92.014115.

Caillard, D., Martin, J.L., 2003. Thermally Activated Mechanisms in Crystal Plasticity. Pergamon.

Carrez, Ph., Ferré, D., Denoual, C., Cordier, P., 2010. Modelling thermal activation of ⟨110⟩{110} slip at low temperature in $SrTiO_3$. Scr. Mater. 63, 434–437.

Castillo-Rodriguez, M., Sigle, W., 2011. The kink-pair mechanism and low-temperature flow-stress behaviour of strontium titanate single crystals. Scr. Mater. 64, 241–244. http://dx.doi.org/10.1016/j.scriptamat.2010.10.014.

Cordier, P., Amodeo, J., Carrez, Ph., 2012. Modelling the rheology of MgO under Earth's mantle pressure, temperature and strain rates. Nature 481, 177–180. http://dx.doi.org/10.1038/nature10687.

Cordier, P., Ungár, T., Zsoldos, L., Tichy, G., 2004. Dislocation creep in $MgSiO_3$ perovskite at conditions of the Earth's uppermost lower mantle. Nature 19, 837–840.

de Wit, R.W.L., Trampert, J., 2015. Robust constraints on average radial lower mantle anisotropy and consequences for composition and texture. Earth Planet. Sci. Lett. 429, 101–109. http://dx.doi.org/10.1016/j.epsl.2015.07.057.

Dorn, J., Rajnak, S., 1964. Nucleation of kink-pairs and the Peierls' mechanism of plastic deformation. Trans. Metall. Soc. AIME 230, 1052–1064.

Ferré, D., Carrez, Ph., Cordier, P., 2007. First principles determination of dislocations properties of $MgSiO_3$ perovskite at 30 GPa based on the Peierls–Nabarro model. Phys. Earth Planet. Inter. 163, 283–291. http://dx.doi.org/10.1016/j.pepi.2007.05.011.

Forte, A.M., Mitrovica, J.X., 2001. Deep-mantle high-viscosity flow and thermochemical structure inferred from seismic and geodynamic data. Nature 410, 1049–1056. http://dx.doi.org/10.1038/35074000.

Fukao, Y., Obayashi, M., Nakakuki, T., the Deep Slab Project Group, 2009. Stagnant Slab: a review. Annu. Rev. Earth Planet. Sci. 37, 19–46. http://dx.doi.org/10.1146/annurev.earth.36.031207.124224.

Girard, J., Amulele, G., Farla, R., Mohiuddin, A., Karato, S.-I., 2016. Shear deformation of bridgmanite and magnesiowüstite aggregates at lower mantle conditions. Science 351, 144–147. http://dx.doi.org/10.1126/science.aad3113.

Glišovic, P., Forte, A.M., Ammann, M.W., 2015. Variations in grain size and viscosity based on vacancy diffusion in minerals, seismic tomography, and geodynamically inferred mantle rheology. Geophys. Res. Lett. 42, 6278–6286. http://dx.doi.org/10.1002/2015GL065142.

Gouriet, K., Carrez, Ph., Cordier, P., 2014. Modelling [100] and [010] screw dislocations in $MgSiO_3$ perovskite based on the Peierls–Nabarro–Galerkin model. Model. Simul. Mater. Sci. Eng. 22, 025020. http://dx.doi.org/10.1088/0965-0393/22/2/025020.

Gröger, R., Vitek, V., 2013. Stress dependence of the Peierls barrier of 1/2⟨111⟩ screw dislocations in bcc metals. Acta Mater. 61, 6362–6371. http://dx.doi.org/10.1016/j.actamat.2013.06.047.

Hirel, P., Krayche, A., Carrez, Ph., Cordier, P., 2014. Atomic core structure and mobility of [100](010) and [010](100) dislocations in $MgSiO_3$ perovskite. Acta Mater. 79, 117–125. http://dx.doi.org/10.1016/j.actamat.2014.07.001.

Hirel, P., Carrez, P., Clouet, E., Cordier, P., 2016. The electric charge and climb of edge dislocations in perovskite oxides: the case of high-pressure $MgSiO_3$ bridgmanite. Acta Mater. 106, 313–321. http://dx.doi.org/10.1016/j.actamat.2016.01.019.

Hirth, J.P., Lothe, J., 1982. Theory of Dislocations. Wiley, New York.

Jónsson, H., Mills, G., Jacobsen, K.K.W., Jonsson, H., 1998. Nudged elastic band method for finding minimum energy paths of transitions. In: Class. Quantum Dyn. Condens. Phase Simulations - Proc. Int. Sch. Phys., pp. 385–404.

Joós, B., Zhou, J., 2001. The Peierls–Nabarro model and the mobility of the dislocation line. Philos. Mag. A 81, 1329–1340. http://dx.doi.org/10.1080/01418610108214444.

King, S.D., 2016. An evolving view of transition zone and midmantle viscosity. Geochem. Geophys. Geosyst. 17, 1234–1237. http://dx.doi.org/10.1002/2016GC006279.

Kocks, U.F., Argon, A.S., Ashby, M.F., 1975. Thermodynamics and Kinetics of Slip. Pergamon Press.

Koizumi, H., Kirchner, H.O.K., Suzuki, T., 1994. Nucleation of trapezoidal kink-pairs on a Peierls potential. Philos. Mag. A 69, 805–820. http://dx.doi.org/10.1080/01418619408242521.

Koizumi, H., Kirchner, H., Suzuki, T., 1993. Kink-pair nucleation and critical shear stress. Acta Metall. Mater. 41, 3483–3493. http://dx.doi.org/10.1016/0956-7151(93)90228-K.

Kraych, A., Carrez, Ph., Hirel, P., Clouet, E., Cordier, P., 2016. Peierls potential and kink-pair mechanism in high-pressure $MgSiO_3$ perovskite: an atomic scale study. Phys. Rev. B 93, 014103. http://dx.doi.org/10.1103/PhysRevB.93.014103.

Kubin, L., 2013. Dislocations, Mesoscale Simulations and Plastic Flow. Oxford University Press.

Liu, X., Zhong, S., 2016. Constraining mantle viscosity structure for a thermochemical mantle using the geoid observation. Geochem. Geophys. Geosyst. 17, 895–913. http://dx.doi.org/10.1002/2015GC006161.

Mainprice, D., 2007. Seismic anisotropy of the deep Earth from a mineral and rock physics perspective. In: Treatise in Geophysics. Volume 2. Mineral Physics, pp. 437–492.

Marquardt, H., Miyagi, L., 2015. Slab stagnation in the shallow lower mantle linked to an increase in mantle viscosity. Nat. Geosci. 8, 311–314. http://dx.doi.org/10.1038/ngeo2393.

Meade, C., Jeanloz, R., 1990. The strength of mantle silicates at high pressures and room temperature implications for the viscosity of the mantle. Nature 348, 533–535.

Meade, C., Silver, P.G., Kaneshima, S., 1995. Laboratory and seismological observations of lower mantle isotropy. Geophys. Res. Lett. 22, 1293–1296. http://dx.doi.org/10.1029/95GL01091.

Merkel, S., Wenk, H.R., Badro, J., Montagnac, G., Gillet, P., Mao, H., Hemley, R.J., 2003. Deformation of $(Mg\ 0.9, Fe\ 0.1)SiO_3$ Perovskite aggregates up to 32 GPa. Earth Planet. Sci. Lett. 209, 351–360. http://dx.doi.org/10.1016/S0012-821X(03)00098-0.

Mitchell, T., Peralta, P., Hirth, J., 1999. Deformation by a kink mechanism in high temperature materials. Acta Mater. 47, 3687–3694. http://dx.doi.org/10.1016/S1359-6454(99)00207-4.

Miyagi, L., 2009. Deformation and texture development in deep earth mineral phases: implications for seismic anisotropy and dynamics. PhD thesis. University of California, Berkeley.

Miyajima, N., Yagi, T., Ichihara, M., 2009. Dislocation microstructures of $MgSiO_3$ perovskite at a high pressure and temperature condition. Phys. Earth Planet. Inter. 174, 153–158. http://dx.doi.org/10.1016/j.pepi.2008.04.004.

Montagner, J.-P., 1994. Can seismology tell us anything about convection in the mantle? Rev. Geophys. 32, 115. http://dx.doi.org/10.1029/94RG00099.

Oganov, A.R., Brodholt, J.P., David Price, G., 2000. Comparative study of quasi-harmonic lattice dynamics, molecular dynamics and Debye model applied to $MgSiO_3$ perovskite. Phys. Earth Planet. Inter. 122, 277–288. http://dx.doi.org/10.1016/S0031-9201(00)00197-7.

Panning, M., Romanowicz, B., 2006. A three-dimensional radially anisotropic model of shear velocity in the whole mantle. Geophys. J. Int. 167, 361–379. http://dx.doi.org/10.1111/j.1365-246X.2006.03100.x.

Peierls, R., 1940. The size of a dislocation. Proc. Phys. Soc. 52, 34–37.

Pizzagalli, L., Pedersen, A., Arnaldsson, A., Jónsson, H., Beauchamp, P., 2008. Theoretical study of kinks on screw dislocation in silicon. Phys. Rev. B 77, 064106. http://dx.doi.org/10.1103/PhysRevB.77.064106.

Plimpton, S., 1995. Fast parallel algorithms for short-range molecular dynamics. J. Comput. Phys. 117, 1–19. http://dx.doi.org/10.1006/jcph.1995.1039.

Proville, L., Ventelon, L., Rodney, D., 2013. Prediction of the kink-pair formation enthalpy on screw dislocations in α-iron by a line tension model parametrized on empirical potentials and first-principles calculations. Phys. Rev. B 87, 144106. http://dx.doi.org/10.1103/PhysRevB.87.144106.

Rudolph, M.L., Lekić, V., Lithgow-Bertelloni, C., 2015. Viscosity jump in Earth's mid-mantle. Science 350, 1349–1352. http://dx.doi.org/10.1126/science.aad1929.

Schoeck, G., 1965. The activation energy of dislocation movement. Phys. Status Solidi 8, 499–507. http://dx.doi.org/10.1002/pssb.19650080209.

Schoeck, G., 2001. The core structure, recombination energy and Peierls energy for dislocations in Al. Philos. Mag. A 81, 1161–1176. http://dx.doi.org/10.1080/01418610108214434.

Seeger, A., Schiller, P., 1962. Bildung und diffusion von Kinken als grundprozess der Versetzungsbewegung bei der messung der inneren reibung. Acta Metall. 10, 348–357. http://dx.doi.org/10.1016/0001-6160(62)90013-5.

Stixrude, L., 2005. Structure and freezing of $MgSiO_3$ liquid in Earth's lower mantle. Science 310, 297–299. http://dx.doi.org/10.1126/science.1116952.

Suzuki, T., Koizumi, H., Kirchner, H.O.K., 1995. Plastic flow stress of b.c.c. transition metals and the Peierls potential. Acta Metall. Mater. 43, 2177–2187. http://dx.doi.org/10.1016/0956-7151(94)00451-X.

Wang, Y., Durham, W.B., Getting, I.C., Weidner, D.J., 2003. The deformation-DIA: a new apparatus for high temperature triaxial deformation to pressures up to 15 GPa. Rev. Sci. Instrum. 74, 3002. http://dx.doi.org/10.1063/1.1570948.

Weertman, J., 1955. Theory of steady-state creep based on dislocation climb. J. Appl. Phys. 26, 1213. http://dx.doi.org/10.1063/1.1721875.

Weidner, D.J., Chen, J., Xu, Y., Wu, Y., Vaughan, M.T., Li, L., 2001. Subduction zone rheology. Phys. Earth Planet. Inter. 127, 67–81. http://dx.doi.org/10.1016/S0031-9201(01)00222-9.

Wenk, H.-R., Lonardeli, I., Pehl, J., Devine, J., Prakapenka, V., Shen, G., Mao, H.-K., 2004. In situ observation of texture development in olivine, ringwoodite, magnesiowüstite and silicate perovskite at high pressure. Earth Planet. Sci. Lett. 226, 507–519. http://dx.doi.org/10.1016/j.epsl.2004.07.033.

Xu, W., Moriarty, J.A., 1998. Accurate atomistic simulations of the Peierls barrier and kink-pair formation energy for ⟨111⟩ screw dislocations in bcc Mo. Comput. Mater. Sci. 9, 348–356. http://dx.doi.org/10.1016/S0927-0256(97)00161-4.

Yamazaki, D., Karato, S.-I., 2001. High-pressure rotational deformation apparatus to 15 GPa. Rev. Sci. Instrum. 72, 4207. http://dx.doi.org/10.1063/1.1412858.